npj | natural hazards

Article

https://doi.org/10.1038/s44304-026-00173-z

Extreme precipitation changes in relation to urbanization

Check for updates

Alice Guccione[1,2] ✉, Paolo Bassi[1], Fabien Desbiolles[3], Matteo Borgnino[1], Fabio D'Andrea[2] & Claudia Pasquero[1]

The rising frequency of extreme precipitation is a major concern linked to climate change, commonly associated with increased atmospheric water vapor due to global warming. In densely populated areas, intense rainfall has particularly severe impacts, with urbanization amplifying extreme weather through changes in land surface and local atmospheric conditions. As attribution science increasingly informs climate policy, it is crucial to discern the extent to which shifts in extreme event probability stem from global versus local anthropogenic drivers. This study analyzes multi-decadal daily precipitation records alongside urbanization indices. In line with previous research, results show a general rise in extreme rainfall frequency, with more intense events exhibiting a larger increase. Analysis of population and urban development metrics reveals that the increase is notably smaller in rural areas, suggesting that the rise attributable to local urban development is of the same order of magnitude as that resulting from global warming. This result is shown to be associated with the urban amplification of convective updraft intensification.

Climate change is causing an increase in extreme precipitation in large portions of the continents[1–4]. The Clausius-Clapeyron (CC) equation dictates an approximate increase in the atmosphere water holding capacity of ~7% for every 1 °C temperature increase under typical near surface atmospheric and pressure conditions, but many deviations from the CC scaling have been observed, depending on the definition of extremes used and the specific characteristics of the regions analyzed[5–7]. A very wide variety of hazards are related to storms and heavy rainfall, all of which can be socially and economically significant. The main impacts include very intense flooding, especially damaging in urban areas[8], outbreaks of waterborne diseases[9], as well as damage or complete collapse of infrastructures[10,11], and the triggering of very fast and disruptive landslides[12]. It is known that urban areas are particularly vulnerable to climate extremes[13] and that urbanization affects rainfall, enhancing mean precipitation by more than 15%[14]. Several different mechanisms linking urbanization to rainfall have been investigated over the last decades. The urban heat island effect is due to increased solar radiation absorption, reduced evaporation, and direct heating by human activities, creating temperature anomalies of up to 10 °C[15], and affects air column stability and boundary layer properties. The urban landscape alters surface roughness and can deviate storm trajectories and modify wind convergence[16,17]. Emissions of pollutants that act as cloud condensation nuclei can modify the microphysical characteristics of clouds, including their life time[18]. The interaction of those complex processes implies that the same urban area can yield different rainfall effects due to environmental factors related to aerosol emissions, enhanced surface moisture content, and synoptic atmospheric characteristics. Previous investigation using observational data and convection-permitting atmospheric simulations in regional and case studies showed that overall urbanization produces an increase in frequency and/or intensity of extremes of daily and subdaily precipitation[19–24]. Recently, moving away from regional investigations and case studies analysis, global assessments of urbanization effects on precipitation were performed[13,25], finding that higher levels of urbanization enhance urban precipitation anomalies.

While there is thus evidence of the effects on extreme precipitation of both global warming and urbanization, research is much needed to assess their relative contributions[26]. Recently, the role of urbanization in exacerbating rainfall produced by tropical cyclones, whose intensity is known to be increasing due to climate change[27], has been quantified in specific case studies[28,29]. Aiming to a similar goal, in this study, we analyze local trends in frequency of extreme daily precipitation and cluster them according to urbanization metrics to quantify differences emerging between the rate of change of occurrence of heavy rainfall between rural and urban areas. The analysis is performed both on a global rain gauge dataset[30,31] for the past 60 years, and for a regional convection-permitting dynamical downscaling of reanalysis data over a 42 year period (CHAPTER[32]).

[1]Department of Earth and Environmental Sciences, University of Milano-Bicocca, Milan, Italy. [2]Laboratoire de Météorologie Dynamique / IPSL, ENS-PSL Université, École Polytechnique-Institut Polytechnique de Paris, Sorbonne Université, CNRS, Paris, France. [3]Institut de Recherches pour le Développement (IRD), Laboratoire d'Études Géophysiques et d'Océanographie Spatiale (LEGOS), University of Toulouse, Toulouse, France. ✉e-mail: a.guccione3@campus.unimib.it

Results

Changes in extreme precipitation occurrence in the global dataset

The daily precipitation data from the Global Historical Climatology Network (GHCNd) has been scrutinized and reduced to retain only data from stations that allow for the computation of reliable extreme precipitation changes over the last six decades, following the procedure presented in[3] and detailed in the Methods section. Despite the large interannual variability of extreme precipitation metrics does not allow for the detection of statistically significant trends for most of the time series from individual rain gauge stations, a general increase of heavy rainfall emerges when the dataset is considered as a whole, as previously discussed[33–35]. When defining extreme events as the 60 most intense daily rainfall recorded at each station (on average, one per year), the average number of occurrences per year computed over the 6028 stations extracted from GHCNd shows a statistically significant trend (Fig. 1b), accounting for a ~20% increase over the 1962–2021 period. The analysis performed on individual stations indicates a net majority of positive slopes in the frequency time series (62.3%), a number that allows the rejection of the null hypothesis of a stationary occurrence of extreme precipitations over the 60 years period at the 95% confidence level.

We further analyze the extreme precipitation time series according to the classification of the station location. To this aim, we use a metric based on population and built-up area density, as developed in the Global Human Settlement Model database[36,37]. The spatial entities used in the database[38], which refer to the urbanization conditions of 2015, are here grouped into three main classes: Urban, Rural, and Water, with the latter comprising only few stations and not further discussed in the following.

The ratio between the number of stations with an increase to that with a decrease in the occurrence of extreme precipitations, clustered among Rural and Urban classes, is shown in Fig. 2e. This ratio is significantly lower for the Rural class (~1.6) than for the Urban class (~2.15). Consistently, the mean increase over the 60 year period analyzed is 19% for Rural station and 29% in the Urban class (Fig. 2f). These results indicate that for Urban stations the increase of extreme precipitation occurrence has been significantly larger than for Rural stations, which constitute the bulk of the data. The statistical tests used to assess the significance of the signals are presented in the Methods section. Some tests have been performed by altering the year to which the GHS_SMOD refers for its urbanization conditions, but no significant differences were found in the results.

A second metric to define urbanization has also been used, based on the distance of the station from densely populated areas. To this aim, an index, referred in the following as "weighted population", is built accounting for the number of inhabitants in the region surrounding the station and weighting it by the distance from the station (see Methods section). The linear regression coefficients for the occurrence of extreme precipitation events in the whole dataset are then clustered into 8 classes with an equal number of stations based on the value of this index. Results, shown in Fig. 2g, h, indicate an increase of the ratio between positive and negative trends with the weighted population index, from ~1.2 in the first bin to ~2.5 in the last, and a corresponding increase of the linear regression coefficient. Stations with a low value of the weighted population index have a marginally increasing occurrence of extreme precipitations (3.6 ± 2.4 % over 60 years), while stations with the highest value of the index experienced on average an increase of 39.1 ± 3.8 % from 1962 to 2021.

In both cases the null hypothesis of no correlation between the frequency trend and the urbanization index can be rejected at the 95 % confidence level: stations in areas within the lower (higher) quartile of weighted population index are associated with a significantly smaller (larger) increase in extreme precipitation frequency compared to the whole set of stations.

A sensitivity study has then been conducted by using different definitions of extreme precipitation events. Rather than selecting the 60 most intense daily rainfall events over the 60 year period under study, a different number of most intense events has been used, ranging from 20 to 240. This corresponds to the use of a different threshold for daily precipitations, from the 98.9th to the 99.9th percentile (60 events correspond to daily rainfall above the 99.7th percentile). This sensitivity analysis reveals that, in general, the relative increase over the entire period is larger for more extreme events, in agreement with[39]. Furthermore, the frequency of extremes in Urban stations increases consistently more than in Rural stations across all percentiles (Fig. 3), with an increasing difference between Urban and Rural values for most intense events. On average, the Urban-Rural difference is on the order of half the change in Rural areas (from 35 to 55%), indicating that the effect of urbanization is of the same order of magnitude, albeit smaller, of the effect of the global driver in extreme precipitation changes.

The presented analysis indicates that the frequency of extreme precipitation events over the last decades has increased more in more urbanized and densely populated areas than in rural and scarcely populated regions, suggesting the existence of a link between changes in heavy rainfall and urbanization. However, it is important to note that part of the global pattern is influenced by the spatial distribution of stations, which unevenly cover a limited portion of Earth's land. As shown in Fig. 2a, b, the Urban category is dominated by stations in North America and (a small portion of Central) Europe, whereas the Rural

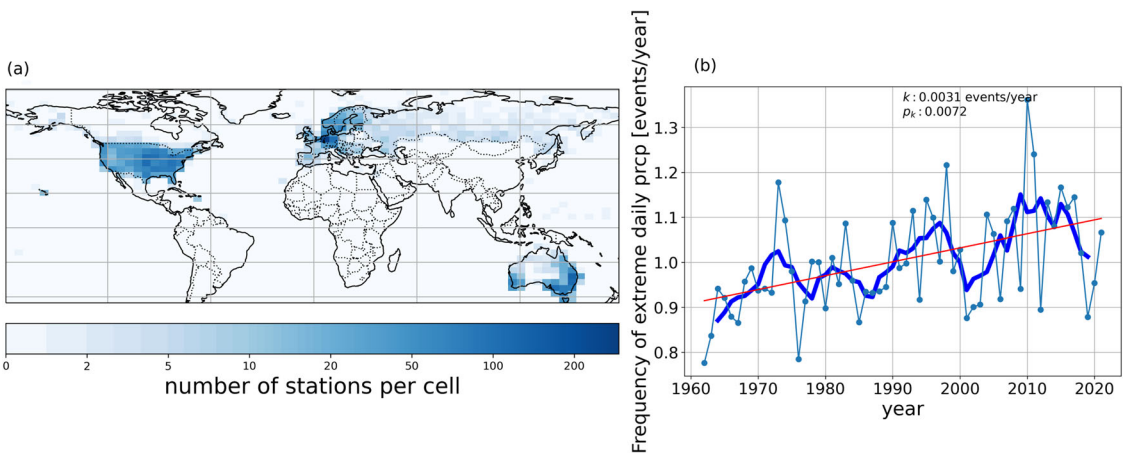

Fig. 1 | Spatial distribution of rain stations and yearly frequency of extreme precipitation. a Spatial distribution of the 6028 selected stations from the GHCNd dataset, shown as number of stations in each 5 x 5 degree box, and **b** mean annual number of extreme daily precipitation events per station over the period 1962–2021, updated from[3]. The bold line represents the five-year rolling mean. In the inset, the linear trend is reported, indicating an increase in frequency of about 20% over the 60-year study period.

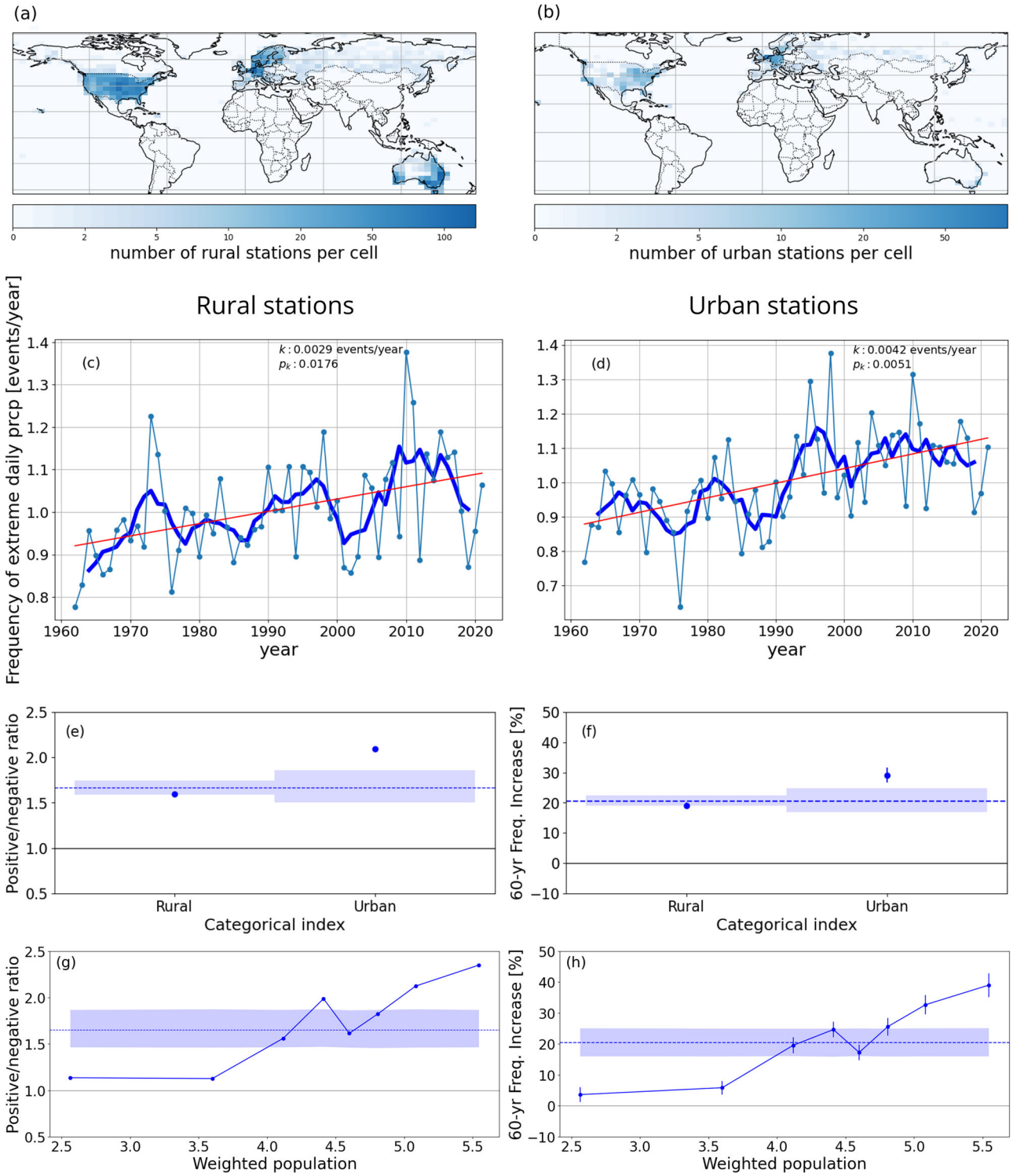

Fig. 2 | Results from analyses on GHCNd precipitation dataset. Spatial distribution of the 6028 selected stations classified as Rural (**a**) and Urban (**b**) according to the categorical index, shown as number of stations in each 5 x 5 degree box. Annual number of extreme daily precipitation events per station averaged across all rural (**c**) and urban (**d**) areas over the period 1962–2021. Trends in frequency of extreme precipitation events versus the categorical index (**e**, **f**) and the weighted population index (**g**, **h**). Results refer to all the selected stations. For each bin the ratio between the number of stations with positive and negative trends (**e**, **g**), and the percent 60-years frequency increase (**f**, **h**) are shown. In (**e**–**h**) the horizontal lines indicate mean values over the whole dataset and shaded areas represent the confidence bands at the fifth and ninety fifth percentiles, obtained by randomly sampling 10,000 times a subset of stations corresponding in size to each class. Error bars in panels d and f reflect, for each bin, the standard error of the mean of slopes propagated using equation (1).

category is mainly contributed by Australia and North America. Although stratifying by region reduces the sample size and no statistically significant result emerges (Fig. S1 in the supporting information), the analysis performed on individual continents shows that there are large differences in the change of extreme event frequency across the globe. For this reason, we cannot rule out the possibility that the signal emerging from the global GHCN dataset stems from large scale regional differences rather than from local land use characteristics. To assess the

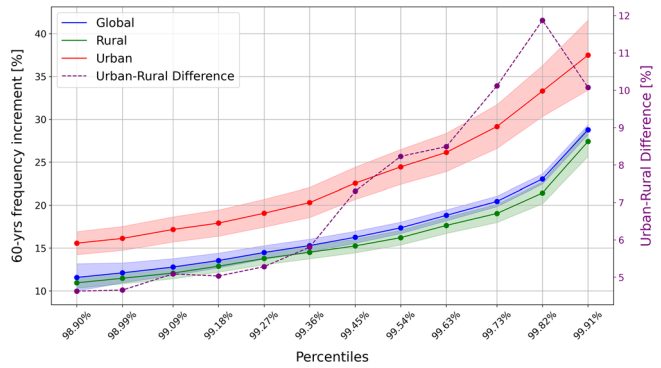

Fig. 3 | Heavy precipitation frequency change over the 1962–2021 period, for different percentiles of precipitations, considering all 6028 stations selected from GHCNd dataset (blue), Urban stations (red), Rural stations (green), based on the categorical index division. Shaded areas indicate the standard error of the percentage, propagated from the mean slope's standard error. The difference between urban and rural values is displayed as a purple dashed line.

spatial homogeneity of the urban-rural signal, we divide the dataset into grid cells. Unlike the previous analysis, which computes trends by averaging across all stations, this approach first calculates mean trends separately for urban and rural stations within each grid cell. These cell-level mean trends are then aggregated at a larger scale, by area-weight averaging them at the continental or global levels, and the urban-rural difference in the 60-yr percentage frequency increase is finally computed. The procedure is repeated using grid cells of different sizes, down to 2° latitude × 2° longitude (shown in Supplementary figures S2 and S3). Despite the heterogeneity emerging at the cell level, in the aggregated results the magnitude of the frequency change is always larger for urban than for rural environments, although the difference is often not statistically significant.

Considering the limited number of stations in the GHCN dataset, which seldom reaches a density of one station per thousand squared kilometers and includes only a small proportion of urban stations, in the next section we present the results of the analysis on a regional dataset to more robustly investigate changes in extreme precipitation frequency at finer spatial scales.

Changes in the extreme precipitation occurrence in the regional dataset

In this section, we report on the analysis on the CHAPTER precipitation dataset[32], obtained using the Weather Research and Forecasting (WRF) dynamical model on a convection permitting 3 km x 3 km grid, covering part of Europe and the Mediterranean region (Fig. 4a), to downscale the ERA5 global reanalysis product[40]. The dataset offers a comprehensive resource for investigating the evolution, drivers, and impacts of extreme weather events at both local and regional scales over the 1981–2022 period[41]. Defining extreme events as the 42 most intense daily precipitation events (an average of one per year) at each grid point, and averaging the obtained time series over the whole domain, a mean increase in the occurrence of extreme events of 7% over the 42 year period is obtained. At individual grid points, the statistical significance of the trends is seldom obtained, but the majority of grid points (58%) has a positive trend.

The separation of grid points according to their categorical index allows us to analyze the change in extreme daily precipitations in Urban and in Rural locations. Results are shown in Fig. 4b-e. The ratio of the number of grid points with a positive to a negative slope is 1.2 for Rural and 1.6 for Urban class (Fig. 4d), in both cases allowing the rejection of the null hypothesis of stationarity that theoretically leads to a ratio equal to 1. The trends computed over the 5 years rolling mean of the time series are positive for both Urban and Rural classes, but the null hypothesis of absence of trend can be rejected at the 95% confidence level only for Urban stations. The increase of the occurrence of intense rainfall events in the 1981–2022 period at Urban locations is more than twice that at Rural locations (+17.8% and + 6.5%, respectively). Once again, the difference between the two classes is statistically significant.

As discussed in the previous section, an important limitation arises from the fact that urban areas are not evenly distributed over the whole domain and thus the different signals emerging from rural and urban zones might be associated to larger scale inhomogeneities.

Discussion

The robustness of the presented results has been evaluated with solid statistical tools. However, the weaknesses of the used datasets and methodologies must be kept in mind. First, the global rain gauge stations have been extracted from the GHCNd database following strict selection criteria. Due to the presence of gaps in the observational time series, this lead to considering a limited number of station data (6028 stations, mainly from USA, part of Europe, and Australia). Clearly, the dataset does not provide a complete cover of the continental areas of our planet. Furthermore, only 1014 stations are in Urban locations, and, as previously discussed, they are not homogeneously distributed in the analyzed regions. Considering that the observed increase in heavy precipitation occurrence differs across geographical areas[3], part of the reported signal can be associated with those inhomogeneities (see also supporting material Fig. S1). For these reasons, the analysis has also been performed on a more compact geographical area, in the European and Mediterranean region, using an available fine scale dataset obtained as a hindcast of ERA5 reanalysis. This approach offers the advantage of enabling comparisons between nearby Urban and Rural locations. However, it may also introduce spatial correlations in extreme precipitation events between adjacent grid points, which can reduce the effective number of degrees of freedom. The downscaling was obtained by numerical integration of a model, in which the presence of Urban areas is parametrized using prescribed soil heat and water capacities and does not allow the discrimination of the effects of different urban landscape features. Despite its simplicity, the model solves energy and water budget equations to compute soil temperature and moisture that affect the land surface fluxes. Further work using more complex land surface models and land cover types could be beneficial for refining the results here presented and to delve into the physical processes responsible for the reported signals. We also note that urbanization is strongly correlated with other characteristics, such as the surface elevation. High altitude areas often present lower populations and fewer buildings, which suggests that further studies should consider a homogeneous dataset in terms of elevation to investigate the dependence on urbanization.

Given the many caveats regarding the analyzed datasets, we propose as a robust way to overcome the limitations associated with statistically insufficient samples of extremes the direct analysis of the underlying physical processes that lead to differences in extreme precipitation trends. CHAPTER provides an ideal framework for such a process-based analysis, and this approach will be pursued in future work. As a first illustrative example, and guided by the fact that most of the selected events occur during summer and fall seasons (Fig. S4)–when mid latitude precipitation is affected by static instability in the air column - we examine trends in convective updraft strength.

The rationale behind this analysis is that urban soils, with their relatively low heat and water storage capacity, tend to destabilize the overlying air column compared to surrounding regions. Rising surface temperatures driven by global warming further enhance the likelihood of strong convective updrafts, an effect that is especially pronounced where the atmosphere is already less stable—namely, over urban areas. CHAPTER data indeed show that trends in the annual mean of maximum updraft velocities exhibit a substantially stronger 42-year increase in urban areas compared to rural regions (see supporting information, Fig. S5). This metric is defined isolating convective events by selecting only maximum vertical velocities exceeding 2 m/s. Annual means are then locally computed over the full CHAPTER domain, and a linear regression is applied to the 42-year time

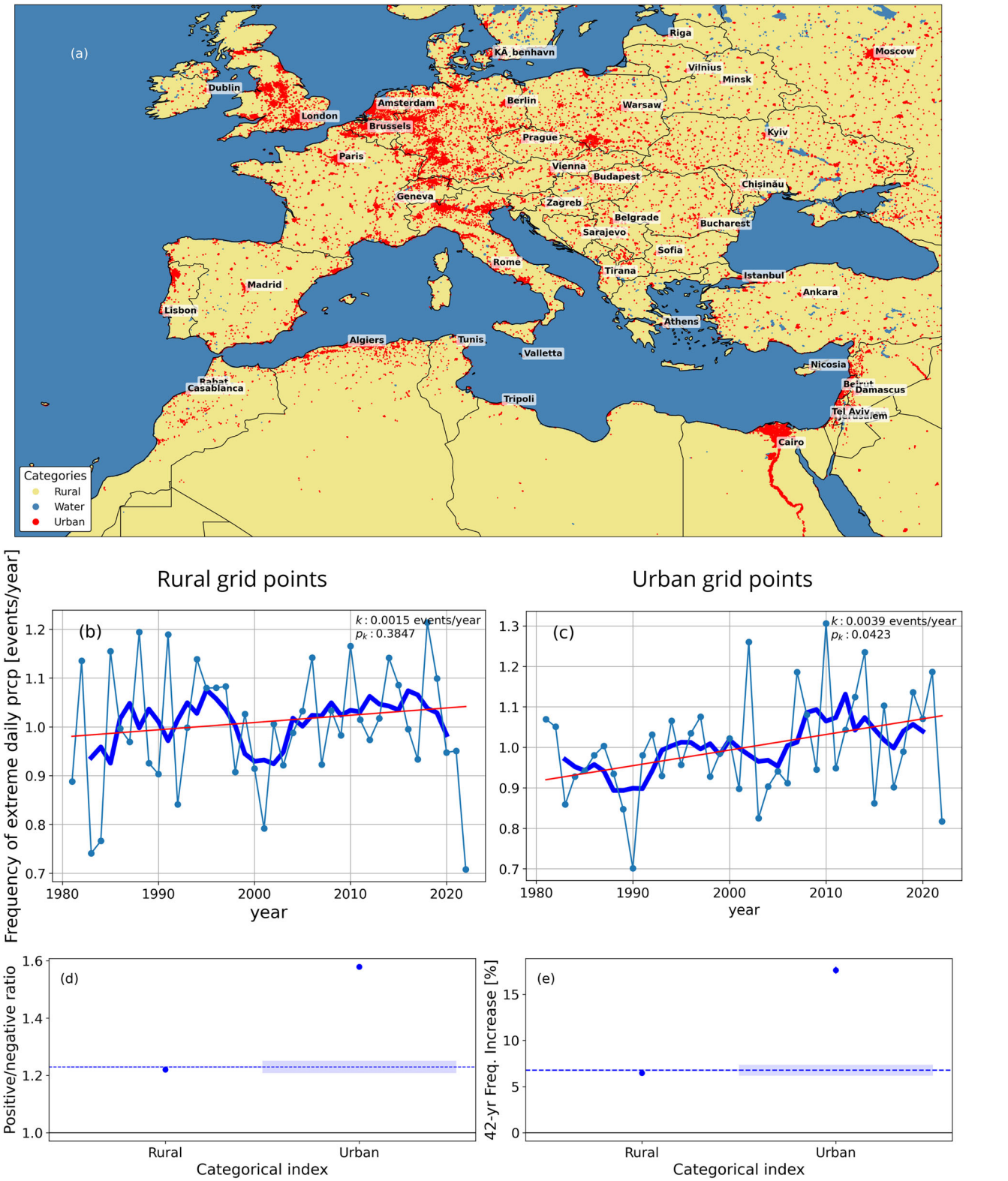

Fig. 4 | Results from analyses on CHAPTER precipitation dataset. a Categorical index in the CHAPTER domain. Annual number of extreme daily precipitation events per grid point averaged across all rural (**b**) and urban (**c**) areas over the period 1981–2022. The bold line represents the five-year rolling mean to which the linear regression is applied. In the inset, the linear trend is reported, indicating an increase in frequency of about 6% over the 42-year study period for rural areas, and about 18% over urban ones. **d**, **e** Trends in frequency of extreme precipitation events. For each category the ratio between the number of stations with positive and negative trends (**d**), and the percent 42-years frequency increase (**e**) are shown. The horizontal lines indicate domain mean values and shaded areas represent the confidence bands at the fifth and ninety fifth percentiles.

series to quantify the trends. The observed pattern indicates that updraft intensification is enhanced over urban land cover, consistent with a local amplification of the increase of convective instability driven by urban-induced effects.

Despite the mentioned limitations of the present study, the reported results show that the probability of heavy daily precipitation exceedance has increased over recent decades, with the most significant rise occurring in urban areas. While the overall rise in extreme rainfall frequency is generally attributed to global warming, the more pronounced increase in densely populated and developed areas is likely linked to differences in land cover.

Findings from this study indicate that, to date, the impacts of the global driver (global warming) and of the local driver (urbanization) have been of the same order of magnitude. Given that heavy precipitation can be particularly problematic in urban areas, and that its occurrence is in a significant part associated with local surface characteristics, our results underscore the need to design urban landscapes in a way that reduces their effects on intense rainfall. This highlights the importance of ongoing and future efforts to identify the most effective urban planning for achieving this goal. Urban areas will likely continue to grow in the future, and understanding how anthropogenic activities alter the local climate is crucial to making cities more resilient to extreme weather.

Methods

Precipitation datasets

The global analysis of precipitation extremes is performed using data sourced from the Global Historical Climatology Network Daily (GHCNd), version 3, an integrated database containing daily climate summaries from land surface stations across the globe. GHCNd is made up of daily climate records from more than 100,000 stations in 180 countries and territories. Its weather stations are screened following the principles described in ref. 3, and the study period (1962–2021) is divided into six decades. This screening results in shrinking the initial ~100,000 stations to 6028 (Fig. 1a). It is clear that the stations are not distributed uniformly across the globe, but they are mainly located in North America, Europe, some parts of Asia, and Australia. The strict selection criteria applied to the dataset limit the analysis primarily to mid-latitude regions.

The regional analysis is conducted on the Computational Hydrometeorology with Advanced Performance to Enhanced Realism (CHAPTER) dataset[32]. It has been obtained as a high-resolution convection-permitting dynamical downscaling of the ERA5 global reanalysis (produced by the European Centre for Medium-Range Weather Forecasts). Briefly, the Weather Research and Forecast (WRF) model has been run on a 3kmx3km grid nested into a domain whose boundary conditions were provided hourly from the ERA5 reanalysis. For each day, the WRF model was initialized at 1800 UTC and run for the following 30 hr. The first 6 hr were considered as spin-up time and thus discarded to obtain daily hindcasts. Having a run starting from ERA5 initial conditions each day prevents the dataset from deviating too much from the large-scale atmospheric condition of ERA5 and justifies why no spectral nudging was used. The soil moisture and temperature fields were initialised with ERA5 hourly data, and the Rapid Update Cycle (RUC) Land Surface Model was used[42,43], with MODIS land cover type dataset derived from the 30-arc-second (roughly 1 km) product (modis_landuse_20class_30s_with_lakes[44]). We note that this database contains several vegetation categories but only one urban and built-up category. Thus, it does not discriminate among different urban landscape features, such as distinct average building heights, but it still computes land-surface fluxes in a different way for urban and rural areas. More information on the CHAPTER dataset and its validation can be found in[41]. In this study, CHAPTER daily accumulated precipitation is analyzed in the 42 year period 1981–2022.

Urbanization indices

Different urban indices are used to characterize the location of the GHCNd stations and of the CHAPTER grid points. We note that different areas could be considered urbanized from certain perspectives but not from others. For instance, in developing countries, a big city might be considered urbanized in terms of population density but not in terms of extensive built up areas or vertical development.

Two different indices have been used: The first one is a categorical index, which consists of a classification of the area linked to its land use and its population density. This classification is taken from the satellite data analyzed in the Global Human Settlement Model layers (GHS_SMOD) database[37], which classifies settlement typologies with a logic of cell clusters based on population and built-up area densities. The GHS_SMOD used in this study, which is relative to the urbanization conditions in 2015, classifies 1 km^2 grid cells based on 8 spatial entities[38]. In this paper, they are further grouped into three main classes: Urban, Rural, and Water. The Urban class is made by Urban Center, Dense Urban Cluster, Semi-dense Urban Cluster, and Suburban spatial entities. The Rural class contains Rural, Low Density Rural and Very Low Density Rural categories. A Water grid cell has at least 0.5 of its surface covered by permanent surface water and is not populated nor built. Each location in both our datasets is then assigned to one of these three categories. Only Rural and Urban classes are used for this study. Overall, only minor differences in classification are observed across the different years available in the GHS-SMOD database (1975, 1990, 2000, 2015, 2020), indicating that the urban/rural assignment is largely stable over time and the potential uncertainty introduced by using a single year as a snapshot is limited and has negligible impact on the results. To further validate this, the analysis has been replicated using the earliest available year (1975). The results are consistent with those based on the 2015 data and remain statistically significant.

The second urbanization index, named weighted population index, is computed as the sum of the populations of the cities around each station, weighted by their distance from it. This index has been calculated using the GeoNames geographical database (https://www.geonames.org/). The algorithm takes the latitude and longitude of each station and searches the GeoNames database for every city within 300 km from the station, selects those with a population of at least 15,000 inhabitants, and then computes the population index as the sum of all populations divided by their distance from the station. Sensitivity analysis has been performed varying the threshold values used in this definition (see supporting information, Figs. S6 and S7). The chosen values are appropriate for the GHCN dataset, which contains lots of stations from areas with isolated cities surrounded by vast rural areas (such as in the United States of America and Australia). For the CHAPTER dataset, the same definition classifies most locations as belonging to the highest classes of weighted population index, given the densely populated European regions. For this reason, and given the very large number of grid points available that gives robustness to the results, we do not use the second metric for the CHAPTER dataset.

Time change metrics and statistical significance evaluation

After constructing the extreme precipitation time series for all the selected stations of the GHCNd and all the grid points over the CHAPTER domain, a rolling mean over a window with size W=5 years is applied. Then, a linear least-squares regression is performed. The resulting trends are examined, with slopes k representing the mean increase in the number of extreme events per year and p-values quantifying their statistical significance, taking into account the temporal correlation of the data (the effective sample size of an annual time series of length N is reduced to (N-W+1)/W). Unless otherwise specified, the confidence level used throughout the paper is 95%. The time changes are either reported as regression coefficients k or expressed as percentage increments over the whole period under study, computed using the following formula:

$$\text{frequency increase over N years (\%)} = \frac{\Delta}{1-\Delta/2} \times 100 \text{ where } \Delta = k \times N \text{ yr} \quad (1)$$

Aggregated analysis is also performed on both the global and regional datasets: the ratio of positive to negative individual slopes is evaluated for each station/gridpoint in the whole dataset and for Urban and Rural categories separately. The null hypothesis of stationarity in the occurrence of extreme daily precipitation is evaluated at 95% confidence level using the binomial distribution. The mean time series of extreme precipitation occurrence and its linear regression over time are also computed for any given group of data. Results are considered to be statistically significant when the p-value of the linear regression is less than 0.05.

For both categorical index and weighted population index we evaluate the significance of the discrepancies obtained in the different classes as follows, based on a Bootstrap test. First, confidence bands are computed using a Montecarlo method: from the whole set of GHCNd stations the algorithm extracts a random subset of size equal to the number of stations in each class and for all extractions it computes both the percentage frequency increase over the 60 years and the ratio between the number of positive and negative slopes; repeating the extraction 10,000 times, histograms of the percentage increment and positive to negative trend ratios are built. The confidence band limits are set at percentiles 5 and 95 of the distributions. Then, stations in a given class are considered to behave differently from the whole dataset if their extreme precipitation metrics lie outside of the 95% confidence band.

Data availability

The data of the Global Historical Climatology Network daily (GHCNd), provided by the National Centers for Environmental Information (NCEI), can be found divided by year at https://www.ncei.noaa.gov/pub/data/ghcn/daily/by_year/.The GHS Settlement Model can be downloaded at https://humansettlement.emergency.copernicus.eu/download.php, selecting the 2015 file. The GeoNames data can be retrieved at http://www.geonames.org/, or through the Python library geonamescache. The CHAPTER dataset is available via the GLOBUS file-transfer service for large-volume data (see http://app.globus.com). Direct link to the dataset on GLOBUS: CHAPTER-public folder on the LRZ DSA Container PN29CO-DSS-0000.

Code availability

The underlying code used for data analysis is available from the corresponding author upon reasonable request. Analyses were performed using Python 3.7.11. Key parameters and variables used are detailed in the Methods section.

Received: 19 September 2025; Accepted: 28 January 2026;
Published online: 09 February 2026

References

1. Westra, S., Alexander, L. V. & Zwiers, F. W. Global increasing trends in annual maximum daily precipitation. *J. Clim.* **26**, 3904–3918 (2013).
2. Donat, M. G., Lowry, A. L., Alexander, L. V., O'Gorman, P. A. & Maher, N. More extreme precipitation in the world's dry and wet regions. *Nat. Clim. Change* **6**, 508–513 (2016).
3. Papalexiou, S. M. & Montanari, A. Global and regional increase of precipitation extremes under global warming. *Water Resour. Res.* **55**, 4901–4914 (2019).
4. Ciarlo', J. & Giorgi, F. An increase in global daily precipitation records in response to global warming based on reanalysis and observations. *Open Res. Eur.* **4**, 114 (2024).
5. Pérez Bello, A., Mailhot, A., Paquin, D. & Paquin-Ricard, D. Temperature-precipitation scaling rates: a rainfall event-based perspective. *J. Geophys. Res. Atmos.* **127**, e2022JD037873 (2022).
6. Martinez-Villalobos, C. & Neelin, J. D. Regionally high risk increase for precipitation extreme events under global warming. *Sci. Rep.* **13**, 5579 (2023).
7. Neelin, J. D. et al. Precipitation extremes and water vapor: Relationships in current climate and implications for climate change. *Curr. Clim. Change Rep.* **8**, 17–33 (2022).
8. Agonafir, C. et al. A review of recent advances in urban flood research. *Water Security* **19**, 100141 (2023).
9. Cann, K., Thomas, D., Salmon, R., Wyn-Jones, A. & Kay, D. Extreme water-related weather events and waterborne disease. *Epidemiol. Infect.* **141**, 671–86 (2013).
10. Nissen, K. & Ulbrich, U. Will climate change increase the risk of infrastructure failures in Europe due to heavy precipitation? *Natural Hazards and Earth System Sciences Discussions* 1–22 (2016).
11. Normand, J. C. L. & Heggy, E. Assessing flash flood erosion following Storm Daniel in Libya. *Nat. Commun.* **15**, 6493 (2024).
12. Tichavsky`, R., Ballesteros-Cánovas, J. A., Šilhán, K., Tolasz, R. & Stoffel, M. Dry spells and extreme precipitation are the main trigger of landslides in central Europe. *Sci. Rep.* **9**, 14560 (2019).
13. Sui, X., Yang, Z.-L., Shepherd, M. & Niyogi, D. Global scale assessment of urban precipitation anomalies. *Proc. Natl. Acad. Sci. USA* **121**, e2311496121 (2024).
14. Liu, J. & Niyogi, D. Meta-analysis of urbanization impact on rainfall modification. *Sci. Rep.* **9**, 7301 (2019).
15. Masson, V., Lemonsu, A., Hidalgo, J. & Voogt, J. Urban climates and climate change. *Annu. Rev. Environ. Resour.* **45**, 411–444 (2020).
16. Pei, Y. et al. Effects of urbanization on extreme precipitation based on weather research and forecasting model: a case study of heavy rainfall in Beijing. *J. Hydrol. Reg. Stud.* **56**, 102078 (2024).
17. He, Y., Wang, J. & Feng, J. A typical weakly forced mountain-to-plain extreme precipitation event exacerbated by urbanization in Beijing. *J. Geophys. Res. Atmos.* **128**, e2023JD039275 (2023).
18. Van Den Heever, S. C. & Cotton, W. R. Urban aerosol impacts on downwind convective storms. *J. Appl. Meteorol. Climatol.* **46**, 828–850 (2007).
19. Yu, M., Liu, Y. & Miao, S. Impact of urbanization on rainfall of different strengths in the Beijing area. *Theoretical Appl. Climatol.* **139** (2020).
20. Li, Y. et al. Strong intensification of hourly rainfall extremes by urbanization. *Geophys. Res. Lett.* **47**, e2020GL088758 (2020).
21. Li, C. et al. Urbanization-induced increases in heavy precipitation are magnified by moist heatwaves in an urban agglomeration of East China. *J. Clim.* **36**, 693–709 (2023).
22. Song, X., Qi, J., Zou, X., Zhang, J. & Liu, C. Potential Effects of Urbanization on Precipitation Extremes in the Pearl River Delta Region, China. *Water* **14**, 2466 (2022).
23. Liang, P. & Ding, Y. The long-term variation of extreme heavy precipitation and its link to urbanization effects in Shanghai during 1916–2014. *Adv. Atmos. Sci.* **34**, 321–334 (2017).
24. Wu, M., Luo, Y., Chen, F. & Wong, W. K. Observed link of extreme hourly precipitation changes to urbanization over coastal south China. *J. Appl. Meteorol. Climatol.* **58**, 1799–1819 (2019).
25. Katzfey, J., Schlünzen, K. H. & Hoffmann, P. Effects of urban areas on the diurnal cycle of temperature and precipitation in a global climate simulation. *Q. J. R. Meteorol. Soc.* **150**, 4885–4914 (2024).
26. Zhang, D.-L. Rapid urbanization and more extreme rainfall events. *Sci. Bull.* **65**, 516–518 (2020).
27. Kossin, J. P., Knapp, K. R., Olander, T. L. & Velden, C. S. Global increase in major tropical cyclone exceedance probability over the past four decades. *Proc. Natl. Acad. Sci. USA* **117**, 11975–11980 (2020).
28. Zhang, W., Villarini, G., Vecchi, G. & Smith, J. Urbanization exacerbated the rainfall and flooding caused by Hurricane Harvey in Houston. *Nature* **563**, 384–388 (2018).
29. Du, X., Chen, H., Li, Q. & Ge, X. Urban impact on landfalling tropical cyclone precipitation: a numerical study of typhoon Rumbia (2018). *Adv. Atmos. Sci.* **40**, 988–1004 (2023).
30. Menne, M. et al. Global historical climatology network–daily (ghcn-daily), version 3.30. *NOAA National Centers for Environmental Information* (2012).
31. Menne, M. J., Durre, I., Vose, R. S., Gleason, B. E. & Houston, T. G. An overview of the global historical climatology network-daily database. *J. Atmos. Ocean. Technol.* **29**, 897–910 (2012).

32. Tartaglione, N., Parodi, A., Bernini, L., Hachinger, S. & Kranzlmüller, D. Chapter: 3x3 km meteorological data 1981-2022 for Europe: 2d extracted fields.[data set]. *Leibniz Supercomputing Centre (LRZ), Garching b.M., Germany* https://doi.org/10.25927/0ppk7-znk14 (2024).
33. Dunn, R. J. H. et al. Development of an updated global land in situ-based data set of temperature and precipitation extremes: Hadex3. *J. Geophys. Res. Atmos.* **125**, e2019JD032263 (2020).
34. Sun, Q., Zhang, X., Zwiers, F., Westra, S. & Alexander, L. V. A global, continental, and regional analysis of changes in extreme precipitation. *J. Clim.* **34**, 243–258 (2021).
35. Intergovernmental Panel on Climate Change. *Climate Change 2023: Synthesis Report* (IPCC, 2023).
36. Eurostat. *Applying the Degree of Urbanisation: A Methodological Manual to Define Cities, Towns and Rural Areas for International Comparisons* (Publications Office of the European Union, Luxembourg, 2021).
37. Schiavina, M., Melchiorri, M., & Pesaresi, M. Ghs-smod r2023a - ghs settlement layers, application of the degree of urbanisation methodology (stage i) to ghs-pop r2023a and ghs-built-s r2023a, multitemporal (1975-2030). *European Commission, Joint Research Centre (JRC)* (2023).
38. Schiavina, M. et al. Ghsl data package 2023 (2023).
39. Fischer, E. M. & Knutti, R. Observed heavy precipitation increase confirms theory and early models. *Nat. Clim. Change* **6**, 986–991 (2016).
40. Hersbach, H. et al. The era5 global reanalysis. *Q. J. R. Meteorol. Soc.* **146**, 1999–2049 (2020).
41. Bernini, L. et al. Convection-permitting dynamical downscaling of ERA5 for Europe and the Mediterranean basin. *Q. J. R. Meteorol. Soc.* **n/a**, e5014 (2025).
42. Benjamin, S. G. et al. An hourly assimilation–forecast cycle: The ruc. *Monthly Weather Rev.* **132**, 495–518 (2004).
43. Smirnova, T. G., Brown, J. M., Benjamin, S. G. & Kenyon, J. S. Modifications to the rapid update cycle land surface model (RUC LSM) available in the weather research and forecasting (wrf) model. *Monthly Weather Rev.* **144**, 1851–1865 (2016).
44. Broxton, P. D., Zeng, X., Sulla-Menashe, D. & Troch, P. A. A global land cover climatology using modis data. *J. Appl. Meteorol. Climatol.* **53**, 1593–1605 (2014).

Acknowledgements

Part of this research was financed by the European Union, Next Generation EU, Mission 4, Component C2, CUP H53D23011300001 (Project LocCLIMA), and by PON Research and Innovation, FSE React-EU, Axis IV, contract C6-G-32370-2, CUP H41B21006270003. This work is an outcome of the project MIUR - Dipartimenti di Eccellenza 2023 - 2027. Rémy Roca is thanked for his valuable insights and assistance. We thank Jost-Diedrich Graf Von Hardenberg, Elisa Palazzi, Olivia Ferguglia, Silvia Caprioli, Nazario Tartaglione and Antonio Parodi for their contributions to our research through fruitful discussions. We are grateful to Lisa Bernini for her help with CHAPTER data management and for helpful discussions.

Author contributions

A.G. performed the analysis, with inputs on technical and statistical aspects from F.D., M.B., C.P., F.D.A. A.G., P.B., F.D., M.B. contributed to code implementation. C.P., F.D.A. conceived the study. A.G. and C.P. wrote the manuscript. All authors discussed the results and commented on the manuscript. All authors have read and approved the manuscript.

Competing interests

The authors declare no competing interests.

Additional information

Supplementary information The online version contains supplementary material available at https://doi.org/10.1038/s44304-026-00173-z.

Correspondence and requests for materials should be addressed to Alice Guccione.